Salt-dissolution faults versus tectonic faults from the case study of salt collapse in Spanish Valley, SE Utah (USA)

Jesús Guerrero[1,*], Ronald L. Bruhn[2], James P. McCalpin[3], Francisco Gutiérrez[1], Grant Willis[4], and Morteza Mozafari[5]

[1]EARTH SCIENCES DEPARTMENT, UNIVERSITY OF ZARAGOZA, 50009 ZARAGOZA, SPAIN
[2]DEPARTMENT OF GEOLOGY AND GEOPHYSICS, UNIVERSITY OF UTAH, SALT LAKE CITY, UTAH 84112, USA
[3]GEO-HAZ CONSULTING INC., 600 E GALENA AVENUE, CRESTONE, COLORADO 81131, USA
[4]1594 WEST NORTH TEMPLE, P.O. BOX 146100, SALT LAKE CITY, UTAH 84114-6100, USA
[5]DEPARTMENT OF EARTH SCIENCES, COLLEGE OF SCIENCES, SHIRAZ UNIVERSITY, 71454, SHIRAZ, IRAN

ABSTRACT

A paleoseismological investigation in Spanish Valley, SE Utah, reveals that faults related to interstratal karstification of salt may show episodic displacement and significantly different parameters than tectonic faults. Spanish Valley is a 25-km-long, 3-km-wide, NW-SE–trending graben formed by the collapse of the crest of a salt anticline. This collapse is related to the karstification of Paleozoic salts, which are several kilometers thick and form the core of the anticline. Differential passive bending of the supra-evaporitic Mesozoic strata produced smaller-scale, NW-SE–trending anticlines and synclines parallel to the axis of the graben on both margins of the collapse valley. Mapping reveals that swarms of synthetic and antithetic normal faults associated with these folds accommodate most of the vertical displacement. A 27-m-long, 4.5-m-deep, trench-like artificial excavation was dug into the hanging wall of the master normal fault of the NE flank with 30–40 m of throw. The excavation exposed a complex structure consisting of a half graben and an asymmetric upper graben separated by a horst. Nine displacement events have been inferred and constrained by consistent AMS (Accelerator mass spectrometry) radiocarbon dates, indicating an anomalously high mean vertical slip rate of 3.07 mm/yr and a very low average recurrence of ~316 yr. The most recent recorded faulting event took place after 2330 cal. yr B.P. Data derived from detailed maps indicate that the faults have aspect ratios (maximum displacement to fault length) comparable to those reported for tectonic faults. However, they show greater aperiodicity, with coefficient of variation values greater than 1, long-term slip rates between 2 and 25 times greater, and displacement per event values up to 30 times higher than those expected for tectonic faults of the same length.

LITHOSPHERE; v. 7; no. 1; p. 46–58; GSA Data Repository Item 2015020 | Published online 11 December 2014 doi:10.1130/L385.1

INTRODUCTION

Seismogenic tectonic faults differ from nonseismogenic tectonic faults in that the former ones are able to cause high-magnitude earthquakes due to sudden slip (episodic motion), while the latter ones are characterized by creep, small slip, and small to moderate earthquakes (McCalpin, 2009a). According to the Nuclear Regulatory Commission, salt-dissolution faults may have significant geomorphic expression, but they are unable to produce significant earthquakes because of their limited rupture area and vertical extent (Huntoon, 1999). Several authors have reported on shallow microearthquakes related to collapse phenomena induced by salt dissolution in different geological contexts (Styles, 2003; Trifu and Shumila, 2010; Dahm et al., 2011; Jousset and Rohmer, 2012; Lenti et al., 2012; Land, 2013).

Mistakenly interpreting nontectonic salt dissolution–induced faults as seismogenic tectonic structures may have important practical implications and lead to seismic hazard overestimates (e.g., Gutiérrez et al., 2012). Evidence of episodic displacement has been proposed as a criterion to differentiate between seismogenic tectonic faults and nonseismogenic salt-dissolution faults in areas underlain by evaporites (e.g., Huntoon, 1999). However, several recent trenching investigations have documented evidence of episodic displacement on normal and flexural-slip faults related to interstratal dissolution of evaporites (Gutiérrez et al., 2012, 2014; Carbonel et al., 2013). Those case studies strongly suggest that episodic faulting is not a reliable criterion for distinguishing between seismogenic tectonic faults and salt-dissolution faulting. Moreover, the work by Gutiérrez et al. (2014) on flexural-slip faults related to evaporite dissolution in the Southern Rocky Mountains of Colorado suggests that, in some cases, such gravitational faults might produce damaging earthquakes (M_w 6); the rupture area of those flexural-slip faults may be as large as 200 km^2. Sudden surface rupture associated with faults characterized by episodic slip is typically recorded by colluvial wedges, fissure fills, and sharp angular unconformities (McCalpin, 2009b). In contrast, cumulative wedge-outs (growth strata) are commonly found in subsidence areas controlled by creeping faults.

Episodic gravitational faulting related to subsurface karstification of soluble rocks may be controlled by a number of interacting factors, including (1) the rate at which evaporites are dissolved by groundwater flow; (2) the extent of the area affected by karstification; (3) the mechanical strength of the strata overlying the karstification zone; and (4) changes in the base level of the hydrogeological system, which may be related to processes like fluvial incision and/or tectonic uplift (Gutiérrez et al., 2012). The intensity of salt dissolution may vary considerably through time, with rates increasing during climatic wet periods, when both groundwater recharge and flow increase (e.g., Berner, 1978; Raines and Dewers, 1997; Jeschke et al., 2001). Other factors that control the solubility and dissolution kinetics of evaporite minerals include temperature (Alkattan et al., 1997; Freyer and Voigt, 2004; McMurry, 2004), effective lithostatic pressure (Blount and Dickson, 1973; Newton and Manning, 2005), pH (Dove and Czank, 1995), the chemistry of the groundwater (Ponsjack, 1940; Wigley, 1973; Ford and

*jgiturbe@unizar.es

Williams, 1989; Alkattan et al., 1997), and the velocity and hydrodynamic regime (laminar vs. turbulent) of the underground flows (Berner, 1978; Raines and Dewers, 1997; Jeschke et al., 2001). Changes in those variables may result in increases or reductions in the dissolution rate, contributing to the episodic behavior of salt dissolution–induced faults. The evolution of karst systems is also sensitive to spatial changes in the subterranean drainage network, such as the opening of new conduits and the collapse of older ones (Ewers and Quinlan, 1981; Ewers, 1982; Birk et al., 2003). Karst systems are also influenced by the spatial and temporal evolution of the surface drainage network. A base-level drop related to fluvial incision or fluvial capture alters the gradient and patterns of the groundwater flow (Palmer, 2000; Lauritzen and Lundberg, 2000).

Even if one assumes steady dissolution under stable groundwater flow conditions, stresses within the overburden change through time and may lead to failure conditions (faulting episodes) when the voids created by karstification reach a critical size and become unstable (Gutiérrez et al., 2008).

Since nontectonic salt-dissolution faults may show episodic behavior like seismogenic tectonic faults, the key question from a diagnostic perspective is: Do salt-dissolution faults have similar scaling and temporal parameters as tectonic faults, such as the aspect ratio of the scarps (height/length), maximum displacement/length ratio (D_{max}/L), slip rate, displacement per event, average recurrence, and recurrence variability?

To our knowledge, this study conducted in Spanish Valley, Utah, is the fourth site where salt dissolution–induced faults have been investigated by trenching and the second one in the United States. The previous sites were located in the Teruel graben (Gutiérrez et al., 2012) and the Cameros Massif (Carbonel et al., 2013) in the Iberian Chain, and the Carbondale collapse center in the Southern Rocky Mountains of Colorado (Gutiérrez et al., 2014). All these studies document evidence of episodic displacement as revealed by colluvial wedges, angular unconformities, upward truncation of faults, and lacustrine deposits indicative of sudden obstruction of drainages related to the rejuvenation of fault scarps. Scaling parameters estimated for some of the evaporite collapse faults in Spain yield D_{max}/L values comparable with those reported for tectonic faults, but higher slip rates, greater displacement per event, and much shorter recurrence than those expected for tectonic faults of the same length and in the same geotectonic setting. Unfortunately, the calculation of parameters for the flexural-slip faults of the Carbondale collapse center, Colorado, was hindered by the poorly constrained chronology of the faulting events.

This paper analyzes the dissolution-induced subsidence structures developed in Spanish Valley on the basis of detailed mapping and characterizes the kinematic behavior of dissolution-induced faults in the area using the full displacement history inferred from a trench dug across the master normal fault on the northeastern margin of the graben.

GEOLOGICAL SETTING

Spanish Valley is a NW-SE–trending graben, 25 km long and 3 km wide, related to the collapse of the crest of a salt anticline in the Canyonlands section of the Colorado Plateau, Utah. The anticline is truncated by the Tertiary diorite laccolith of the La Sal Mountains and crossed transversely by the Colorado River (Fig. 1). The valley forms part of a suite of collapsed salt-cored anticlines in the Paradox fold-and-fault belt of Utah and Colorado. From NE to SW, these dissolution-induced grabens are Fisher Valley, Sinbad Valley, Salt-Cache Valley, Castle Valley, Paradox Valley, Spanish Valley, Gypsum Valley, and Lisbon Valley (Fig. 1). Spanish Valley is situated in the central and deepest part of the ancestral evaporitic Paradox Basin, which developed along the southwestern flank of the Uncompahgre uplift during middle Pennsylvanian to Middle Permian time in Utah and Colorado (Stevenson and Baars, 1986). The ancestral Uncompahgre uplift was a 50-km-wide, NW-SE–trending, basement-involved arch, bounded on both margins by 200–300-km-long fault zones (Barbeau, 2003). The Paradox Basin was interpreted as a pull-apart basin by Stevenson and Baars (1986), but Barbeau (2003) concluded that it was an intraforeland flexural basin adjacent to the Uncompahgre uplift. The Pennsylvanian-age evaporitic Paradox Formation records 29 distinct cycles of halite (Hite, 1960). During the Permian, the salt underwent lateral and upward flow, presumably favored by faulting and differential loading related to thickness variations in the overburden. This halokinetic activity led to the development of NW-SE salt-cored anticlines above Proterozoic basement fault lineaments, and intervening subsidence troughs (Cater, 1970; Stevenson and Baars, 1986; Doelling, 1988, 2000). The salt-bearing Paradox Formation was originally 1200 m thick (Cater, 1970), but it reaches up to 3500 m in thickness along the salt walls that form the core of the anticlines (Baars and Doelling, 1987). Structural and stratigraphic relationships (e.g., thickness variations of stratigraphic units across the anticlines) reveal that salt flowage continued over ~100 m.y. during the Triassic, Jurassic, and Early Cretaceous, when the region became an inland sea with deposition of the Cretaceous Mancos Shale (Baars and Doelling, 1987; Doelling 1988, 2000). During the Late Cretaceous–Early Tertiary Laramide orogeny, the region underwent west-to-east tectonic shortening that reactivated the preexisting structures (Baars and Stevenson, 1981; Pevear et al., 1997). The Oligocene diorite laccolith of the La Sal Mountains intruded into the terrain at around 29 Ma (Doelling, 2000). Fluvial incision associated with the regional uplift of the Colorado Plateau started around 5–6 Ma (Hoffman et al., 2011), and it is still continuing (Pederson et al., 2013a, b). The consequent continuous base-level drop enhanced the circulation of groundwater through deeper strata, favoring interstratal karstification of the Paradox Formation (Cater, 1970; Doelling, 2000; Gutiérrez, 2004).

The sedimentary succession exposed in the studied sector of Spanish Valley ranges from leached evaporites of the middle Pennsylvanian Paradox Formation (cap rock) to the Cretaceous Mancos Shale. Drilling data indicate that the Paradox Formation has a minimum thickness of 1500 m in Spanish Valley (Doelling, 2001). The salt-rich beds grade upward into a karstic residuum, more than 250 m thick, devoid of salt and mainly consisting of highly distorted calcium sulfates and shales. This cap rock crops out along the valley margins as jumbled masses of contorted and brecciated gypsum, black shale, and dolomite beds affected by halokinetic flow and dissolution-induced collapse (Fig. 2A; Doelling, 2001).

Triassic (Moenkopi and Chinle Formations) and Lower Jurassic rocks (Wingate, Kayenta, and Navajo Formations) overlie the Paradox Formation along both flanks of the valley. Middle and Upper Jurassic and Cretaceous formations are only exposed at the southeastern end of the valley. The Mesozoic formations dip 15°–30° away from the collapsed core of the anticline, attaining a subhorizontal attitude several hundred meters away.

The Spanish Valley graben changes abruptly at its NW edge into a half graben controlled by the 45-km-long, NE-dipping Moab fault, located on the SW margin of the depression (Fig. 2A; Foxford et al., 1996). Doelling (2001, 2004) proposed that this fault extends along the axis of Spanish Valley and could be related to both salt dissolution and extensional tectonics (Berg and Skar, 2005). The Moab fault offsets a 5000-m-thick sequence of Carboniferous- to Cretaceous-age rocks with a maximum dip-slip displacement of 950 m (Foxford et al., 1996). Displacement along this listric fault formed a SW-verging, asymmetric roll-over anticline (Moab anticline) in the hanging wall (Garden et al., 2001). No evidence of Quaternary activity has been found associated with the Moab fault (Olig et al., 1996; Wong et al., 1996). From K-Ar analysis of clay gouge along the northern section of the Moab fault, Pevear et al. (1997) reported that the last faulting period occurred ca. 50–60 Ma. Garden et al. (2001) indicated that hydrocarbon migration in the Moab anticline associated with motion

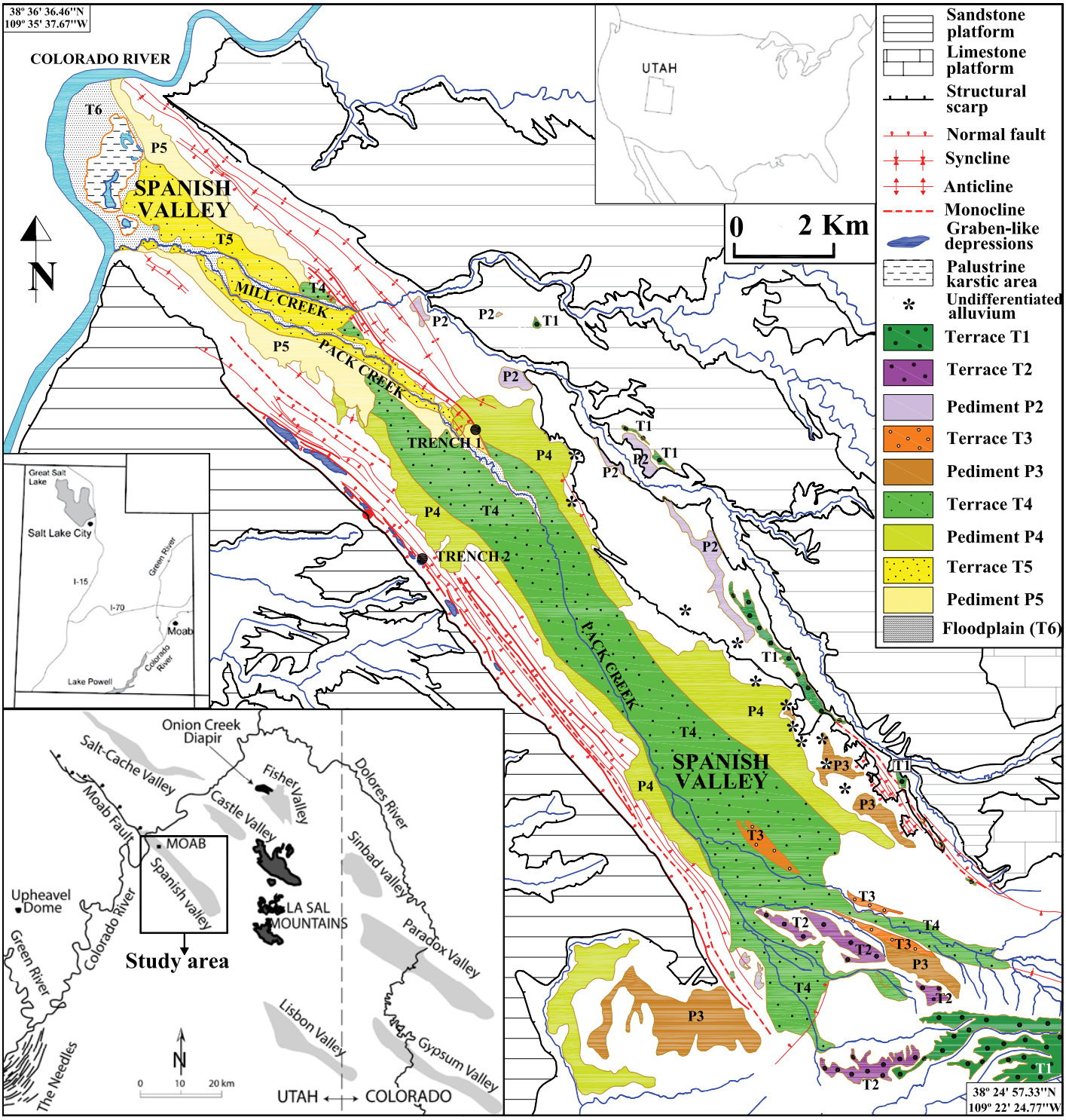

Figure 1. Geological context and geomorphological map of Spanish Valley. Black dots indicate locations of trenches. Primary faults are shown with thicker lines.

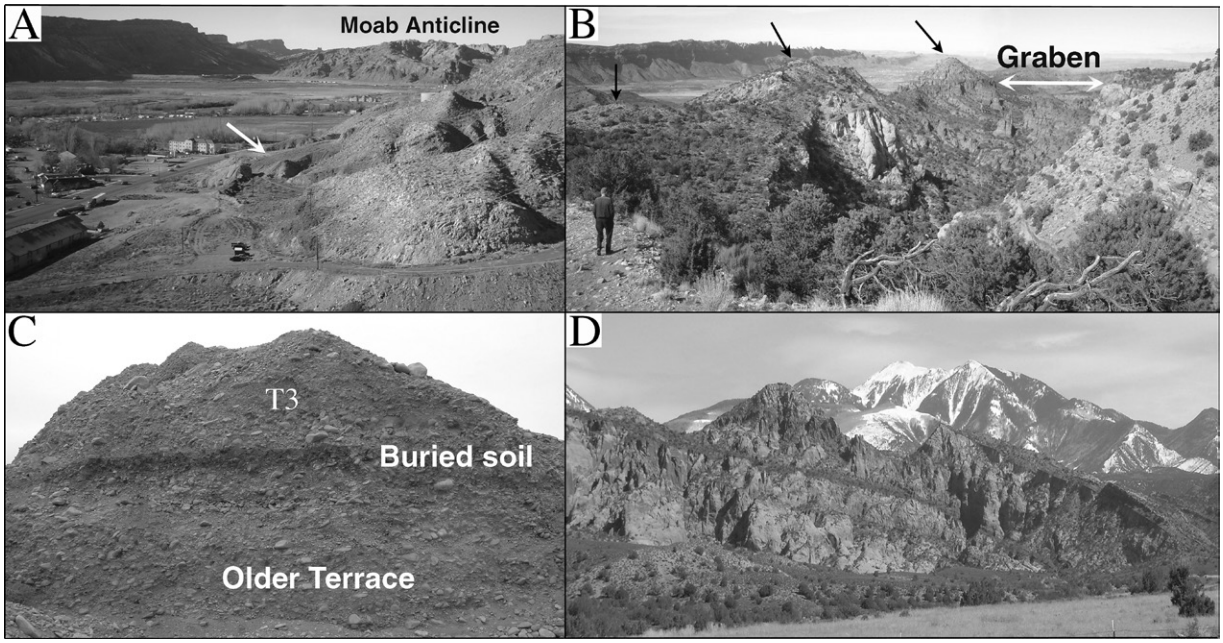

Figure 2. (A) General view of the NW sector of Spanish Valley, which changes into a half graben with a roll-over anticline (Moab anticline) controlled by the Moab fault (background). Paradox Formation (white arrow) crops out at the NE margin of the valley. Image taken from 38°35′09.95N, 109°32′37.76W. (B) Graben structure at the southeastern end of the valley, looking northwest. The Mesozoic sequence is capped by 7–10 m of T1 terrace deposits (black arrows), suggesting that the dissolution-induced collapse of the valley started after the development of T1. Taken from 38°27′19.13N, 109°22′43.24W. (C) Exposure in a gravel pit showing T4 terrace deposits overlying an older alluvial unit with a well-developed dark-brown buried soil on top. Taken at 38°29′16.57N, 109°27′15.88W. (D) Broad monoclinal fold in Navajo Sandstone at the southeastern end of Spanish Valley. View is to the east with the La Sal Mountains in the background. Taken from 38°28′30.09N, 109°25′36.16W.

on the fault occurred at 65 Ma. Dating of neoformed illite and illite-smectite samples by $^{40}Ar/^{39}Ar$ in fault gouge and adjacent rocks yielded ages between 60 and 63 Ma (Solum et al., 2005). Thus, the last period of major activity on the Moab fault presumably dates back to the Laramide orogeny (Pevear et al., 1997; Garden et al., 2001; Solum et al., 2005). Furthermore, there is no microseismicity associated with the Moab fault. Most seismicity occurs along a NE-trending Precambrian basement fault zone along a 35-km-long stretch of the Colorado River southwest of Spanish Valley (Wong and Simon, 1981; Wong et al., 1996).

The timing of salt dissolution and collapse of the anticline crest in Spanish Valley is poorly constrained because of: (1) the scarcity of stratigraphic and geomorphic markers of Cenozoic age; (2) the limitations of the correlations of deposits based on the morphological stage of petrocalcic horizons; and (3) the limited optically stimulated luminescence (OSL), radiocarbon, and paleomagnetic dating. The oldest preserved alluvial deposit, T1 (Fig. 1), probably of glaciofluvial origin (Woodward-Clyde Consultants, 1980; Harden et al., 1985), occurs as a perched unit on the eastern flank of Spanish Valley, situated at 240 m above the depression floor (Fig. 2B). The deposit has reversed paleomagnetic polarity (Biggar et al., 1981), suggesting it is early Pleistocene–late Pliocene in age. This evidence suggests that the collapse of the valley started during or after the deposition of the alluvial unit T1.

GEOMORPHOLOGICAL SETTING

Spanish Valley is bounded by 300–450-m-high vertical cliffs that are underlain by massive sandstone of the Jurassic Wingate and Navajo Formations (Fig. 1). Rock slides, rockfalls, and topples are responsible for cliff retreat, and the resulting deposits accumulate in the lower debris-covered slopes developed on less resistant Triassic bedrock. At the foot of the slopes, there is a sequence of mantled pediments that grade into axial terraces along the valley bottom, where the cover deposits mantle residual cap rock and foundered bedrock blocks. We mapped a stepped sequence of six terrace levels (T1 to T6; from oldest to youngest) belonging to Mill Creek and Pack Creek that drain the valley longitudinally, and four levels of mantled pediment correlative to some of the terraces (P2, P3, P4, P5; Fig. 1). The alluvium of terraces T1 to T4 (older terraces) consists of 7–10 m of poorly sorted, crudely stratified, boulder and cobble gravel with sand matrix. The pedogenic calcic horizons developed on these terrace deposits display continuous carbonate (stage III) or laminated carbonate (stage IV) depending on the locality (Biggar et al., 1981). Terraces T5 and T6 (younger terraces) are mainly composed by 2.5–4 m of sand and silt with some lenticular gravel beds.

There are three lines of geomorphic evidence indicating that dissolution-induced subsidence has been active in Spanish Valley since the Pleistocene:

(1) According to Harden et al. (1985), the longitudinal profiles of the older terraces display a continuous downstream gradient decrease and disappear at the southeastern reach of the graben. Thus, older terraces converge in the graben to form a thickened alluvial deposit made up of superimposed terrace fills. The presence in the middle sector of Spanish Valley of a complex pattern of buried soils (Fig. 2C), and stacked alluvial units beneath terrace T4 support Harden's et al. hypothesis that thickened deposits correlative to older terrace levels lie beneath younger terraces. This stratigraphic relationship should be related to dissolution-induced synsedimentary subsidence, as reported in other fluvial systems developed on halite-bearing evaporates (Guerrero et al., 2008, and references therein).

(2) According to Smith and Goodknight (2005), although gravel strath terraces exist along the canyon carved by the Colorado River both upstream

TABLE 1. RADIOCARBON DATES OF TRENCH 1 SAMPLES

Sample number	Laboratory number	Material	Sedimentology/layer	Conventional ^{14}C age (yr B.P.)	2 sigma calibrated age (yr B.P.)
Moab_0_SW	Beta—299921	Charcoal	Colluvium/2	4010 ± 30	4500–4490
Moab_1_down	Beta—300144	Organic sediment	Peat/4	3940 ± 30	4340–4290
Moab_1_up	Beta—301190	Organic sediment	Peat/4	3150 ± 30	3400–3330
Moab_2_SW	Beta—301188	Wood	Sand/4	1390 ± 30	1320–1270
Moab_3_NE	Beta—301189	Charcoal	Sheetwash deposit/6	2410 ± 30	2680–2640
Moab_4_NE	Beta—301193	Charcoal	Sheetwash deposit/6	2390 ± 30	2460–2340
Moab_5_SW	Beta—301192	Organic sediment	Peat/7	2390 ± 30	2460–2340
Moab_7_NE	Beta—301191	Charcoal	Sheetwash deposit/8	2340 ± 30	2360–2340
Moab_9_NE	Beta—301194	Charcoal	Sheetwash deposit/12	2230 ± 30	2330–2140

Note: Organic sediment refers to total organic carbon (bulk carbon) remaining in the <180 μm size mineral fraction after removal of any carbonates and rootlets.

and downstream of Spanish Valley, the absence of Colorado River terraces in the graben is due to the superposition of fluvial fills caused by salt-dissolution subsidence. The log of a borehole drilled at the northern end of the graben (just outside the study area) reveals more than 120 m of fluvial gravels and sands resting on cap rock, recording an intense and sustained synsedimentary subsidence.

(3) The presence of ponded subsidence depressions up to 1.3 km^2 in the Colorado River floodplain, where the water table intersects the topographic surface ("palustrine karstic areas" in Fig. 1), indicates a karstic subsidence rate higher than river aggradation.

METHODOLOGY

The investigation started with the production of a preliminary map of the study area based on the interpretation of color stereoscopic aerial photographs printed at 1:24,000 scale, and the review of published geological information. The geological maps of Spanish Valley produced by Doelling (2001, 2004) and Doelling et al. (2002) constituted highly useful documents for the characterization of bedrock geology. Special attention was paid to the distribution of fault scarps and faulted Quaternary deposits as targets for the trenching investigation. In a subsequent phase, the map was refined in the field using color 1:10,000 scale orthophotographs.

The trenches were oriented perpendicular to the strike of the faults. We followed the procedure for logging paleoseismological trenches as described by McCalpin (2009a). After cleaning the trench walls, a reference grid with horizontal and vertical strings spaced 1 m apart was placed on the shaded side of the trench, which was then logged on graph paper at a scale of 1:50. Material datable by the radiocarbon method (peat, charcoal, and pieces of wood within silt or sand deposits) was collected from the excavated deposits, preferably in the units situated at the base of the graben fill and in those located just beneath and above the stratigraphic discontinuities recording faulting events (event horizons). The retrodeformational analysis of the trenches was conducted using Autocad 2008. The samples were dated at Beta Analytic, Inc., in Miami, Florida, using accelerated mass spectrometry (AMS), and the ages were calibrated using the INTCAL 04 calibration curve of Reimer et al. (2004) (Table 1).

MORPHOSTRUCTURAL FEATURES OF SPANISH VALLEY

Dissolution-induced subsidence in the crest of the salt anticline has been accommodated by both passive bending (folding) and collapse (normal faulting). The downdropped supra-evaporitic sediments are buried by more than 100 m of alluvium in the bottom of the Spanish Valley, concealing the subsidence structures (Smith and Goodknight, 2005). However, exposures along the flanks of the valley allow us to observe the deformation structures and infer the mechanism involved in the subsidence. Differential sagging in the Mesozoic formations caused by intrastratal karstification of the Paradox Formation produced a sequence of NW-SE–trending anticlines and synclines exposed on both margins of the valley. The folds have wavelengths from 50 to 400 m and lengths in excess of 17 km. Swarms of synthetic and antithetic normal faults within the folds accommodate most of the vertical displacement. Synthetic faults have throws of more than 80 m, while vertical separation on antithetic faults is mostly between 5 m and 20 m and never exceeds 30 m. Locally, the dissolution-induced deformation has generated complex structures in which the strike and dip of the strata change significantly over short distances. According to Cater (1970), the initial radius of curvature of the folds controlled deformation within the salt anticlines. Open anticlines favored ductile deformation (passive bending), whereas subsidence was mainly accommodated by brittle collapse (normal faulting) in tighter anticlines with shorter radius of curvature.

The subsidence magnitude attenuates toward the southeastern end of the valley, where the number of normal faults, their throw, and the dip of the fold limbs gradually decrease, to form single monoclines with dips in the limbs of 20°–30° on both flanks of the valley (Fig. 2D). These paired monoclines terminate at a WNW-ESE–trending syncline (Pack Creek syncline) and a NE-trending fault system developed in Jurassic and Cretaceous rocks that are partially covered by alluvial deposits (Doelling, 2004).

When considered in detail, the amount and structural style of subsidence differ slightly along both margins of Spanish Valley. On the NE flank, the Mesozoic strata exhibit several gentle to open anticlines and synclines with limb dips ranging from 5° to 40° (Fig. 3A). Locally, the folds are affected by graben structures along their hinges up to 1 km long and 100 m wide, controlled by subvertical synthetic and antithetic normal faults. Two nearly vertical normal faults, 5 km and 1.6 km long, accommodate most of the deformation where Mill Creek enters Spanish Valley (Fig. 1). Both faults juxtapose the Kayenta and Navajo Formations. We have estimated a minimum vertical separation of 30 m based on outcrop thickness of Navajo Sandstone in the hanging wall. The easternmost fault is associated with the collapse of the hinge of a syncline, while the fault closest to the valley is related to collapse of the SW limb of a SW-verging anticline (Fig. 3B). In the downthrown block, terrace deposits of Pack Creek and Mill Creek reach more than 30 m thickness and are offset by multiple normal faults (see section 2 of Data Repository data[1]).

[1]GSA Data Repository Item 2015020, description of the sedimentology and spatial distribution of undifferentiated alluvium, paleoseismological study of gravitational structured recorded in Pack Creek terraces and extended explanation of the stratigraphy and structure of trenches 1 and 2, is available at www.geosociety.org/pubs/ft2015.htm, or on request from editing@geosociety.org, Documents Secretary, GSA, P.O. Box 9140, Boulder, CO 80301-9140, USA.

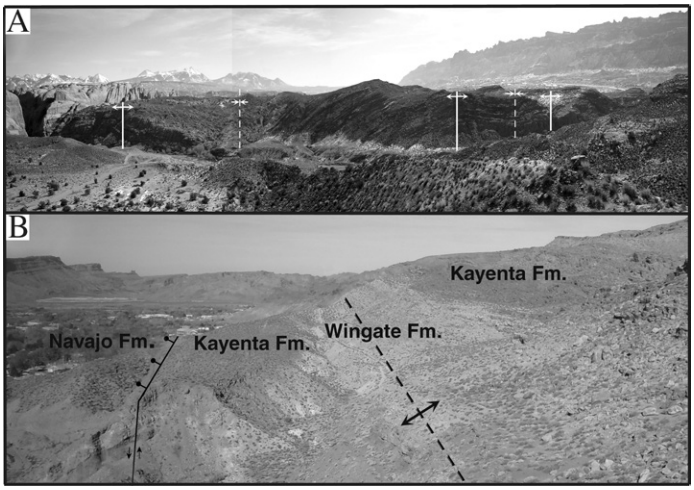

Figure 3. (A) Sequence of open anticlines (solid lines) and synclines (dashed lines) in Navajo and Kayenta Formations at the northeastern margin of Spanish Valley. View is to the east, with the La Sal Mountains in the background. Taken from 38°33′56.15N, 109°31′03.56W. (B) Normal fault developed on the SW limb of a tight anticline (axis indicated by dashed line) that juxtaposes the Navajo Sandstone against the Kayenta Formation. View is to the northwest from 38°33′28.40N, 109°31′11.08W.

Subsidence is apparently greater on the SW flank of Spanish Valley. Ductile downwarping and brittle collapse of the competent Mesozoic sandstone beds created a sinuous monocline, 17.6 km long, at the upper part of the valley wall. The crest of the monocline is cut by a keystone graben that is 15.5 km long and 150 to 350 m wide with conspicuous geomorphic expression (Fig. 4A). The keystone graben is bounded by a master, NE-dipping synthetic fault and a swarm of secondary antithetic, SW-dipping faults with en-echelon arrangement that are connected by relay ramps in the step-over zones (Fig. 4B). Throw on the synthetic fault is between 90 m and 150 m in the central sector of the valley and decreases progressively toward both ends. In contrast, the antithetic faults are 150 m to more than 1300 m in length, i.e., considerably shorter than the master synthetic fault. The throw on these secondary faults is 5–45 m and is expressed by sackung-like uphill-facing scarps up to 30 m high. On the upslope side of the fresh-looking antislope scarps, there are elongated enclosed depressions, 150–950 m long and 45–115 m wide, that behave as sediment traps filled by colluvium, slope wash, and eolian deposits (Figs. 4B and 4D). Some of these fault-controlled depressions have been breached by the drainage network, creating deep gullies that expose a Quaternary graben fill up to 20 m thick. Extension has also produced linear fissures up to 90 m long and 3 m wide along the master synthetic fault scarp (Fig. 4A). Cover suffosion and cover collapse sinkholes up to 7 m and 2 m in diameter, respectively, are also relatively common along the trace of the fissures. Their formation is attributed to the downward migration (raveling and piping) of trough-filling deposits through open fissures in the bedrock. Trench 2 was dug across the scarp associated with a 350-m-long antithetic fault that offset Quaternary trough-filling deposits (section 4 of Data Repository data [see footnote 1]).

In the northeaster limb of this monocline, a shorter and shallower linear graben, more than 6 km long and up to 145 m wide, caused the collapse of Kayenta beds into Wingate strata, with a minimum vertical displacement of 30 m. Despite the intense deformation, the graben is strongly dissected by the drainage network, and fault scarps are degraded, indicating limited or no current activity. The fact that faults are more active and show more recent activity at the marginal sectors of the valley suggests that gravitational deformation migrates away from the valley axis, with a consequent increase in valley width.

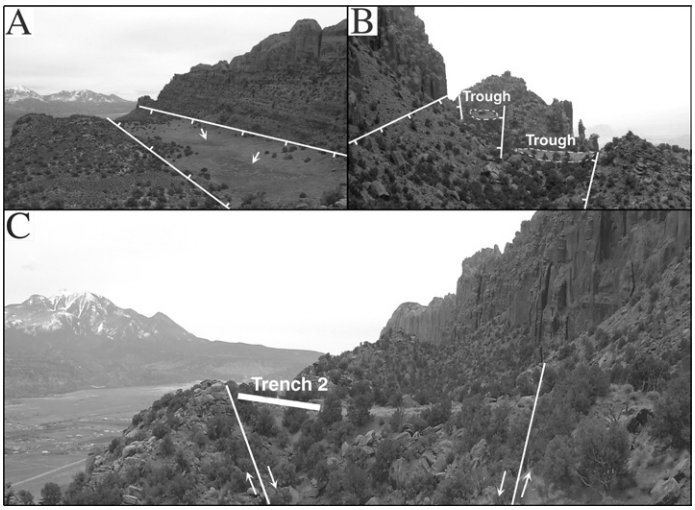

Figure 4. (A) Keystone graben on the SW margin of Spanish Valley, looking south. Arrows point to enclosed troughs in the floor of the depression. Photo taken from 38°32′35.25N, 109°32′37.70W. (B) Swarm of secondary antithetic faults with en-echelon arrangement that control the development of flat-bottom alluvium and eolian-filled troughs. Photo taken from 38°30′36.91N, 109°30′13.81W. (C) Location of trench 2 excavated across a secondary antithetic fault in a marginal keystone graben. Photo taken from 38°31′00.53N, 109°30′31.57W.

TRENCHING STRATIGRAPHY AND GEOCHRONOLOGY OF DEFORMATION EVENTS

Two trenches were excavated across faults that offset Quaternary deposits on both margins of Spanish Valley (see location in Fig. 1). Trench 1 explores the main fault on the NE margin of the valley where it offsets Pack Creek terrace T5 deposits. Trench 2 was dug across an antislope scarp related to a secondary antithetic fault in a marginal graben depression on the SW margin of the valley (Fig. 4C). The log of trench 1 is presented in this section because it records a protracted faulting history constrained by AMS radiocarbon dates. The information related to trench 2, from which no numerical dates were obtained, is included in section 4 of the Data Repository (see footnote 1).

Trench 1

Trench 1 was a 27-m-long, 4.5-m-deep excavation located at 38°32′20.11N, 109°29′42.78W that exposed the longest fault mapped on the NE margin of Spanish Valley (Fig. 1). This trench corresponds to a preexisting artificial excavation from the 1950s that was improved using hand tools. The fault has a cartographic length of 5 km and a minimum throw of 30 m in its central sector, where the Navajo Sandstone is juxtaposed against Kayenta Formation (Fig. 5A). The trench was oriented N060E and located close to the SE edge of the mapped trace of the fault. At the trench site, the deposits of Pack Creek T5 terrace are deformed and in fault contact with Navajo Sandstone (Fig. 5B). This Quaternary fault is expressed in the landscape as a 5-m-high fault scarp (Fig. 5C). The fault splays into three smaller branches 100 m to the southeast of the trench site and then disappears under Pack Creek floodplain deposits. Several springs occur

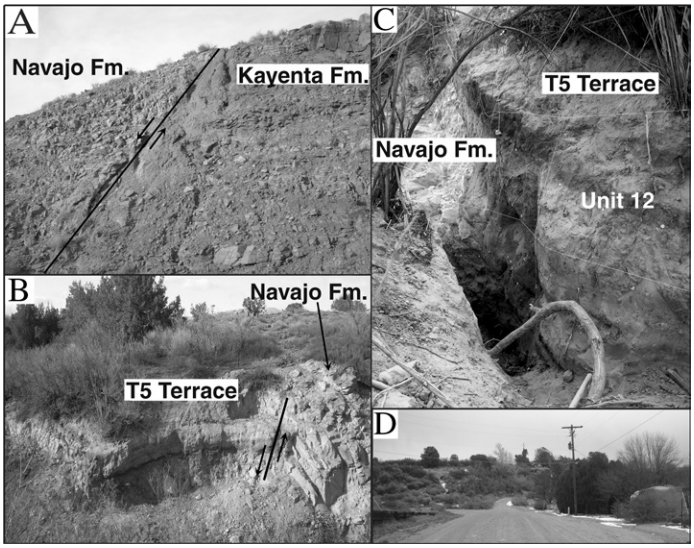

Figure 5. (A) Outcrop of the main fault mapped on the NE margin of Spanish Valley and investigated in trench 1, where brecciated Navajo Sandstone is juxtaposed against broken up Kayenta Formation. Photograph taken at 38°33′28.34N, 109°31′09.81W. (B–C) Overview of the upper half graben and downthrown block of trench 1 showing the deposits of Pack Creek terrace T5 in fault contact with Navajo Sandstones, respectively. (D) Fault scarp, 5 m high, on Pack Creek T5 deposits at the bottom of the valley. Photograph taken from 38°32′20.25N, 109°29′42.46W.

at the foot of the fault scarp (Fig. 5C), supporting the growth of bushes and trees. Calcite, quartz, goethite, and manganese oxides cement the fault zone. Finally, the trench location near the tip of fault implies that the measured displacements and slip rates have to be taken as minimum values.

The trench exposed 18 sedimentary units and a horst and graben structure affecting Holocene deposits in the hanging wall of the mapped fault. The mapped structure comprises an intermediate bedrock horst flanked by an upper graben, 9 m wide, and a downthrown block to the west (Fig. 6). Section 3 of the Data Repository (see footnote 1) includes a detailed description of the stratigraphic units and the deformation structures. In total, nine samples collected from key stratigraphic units were dated by the AMS radiocarbon method (Table 1). The upper graben includes a tapering-downward fissure (unit 17) that is 42 cm wide at the top (Figs. 7A and 7B) and eight subvertical faults (F10 to F17). F10 shows a 2.30-m-wide shear zone. The downthrown block west of the horst is bounded by the synthetic master fault F7, dipping 50°SW (Fig. 6). The subvertical faults F1 to F6 constitute a splay of secondary failure planes emanating from fault F7. Displacement on faults F7 and F5 is responsible for the folding of units 4–13, the deposition and dragging of two colluvial wedges with thicknesses of 77 cm and 48 cm thick (Figs. 7C and 7D), respectively, and complex soft sediment deformation in the sandy unit 4.

The structural and stratigraphic relationships observed in the trench, together with the available numerical dates, allow us to infer a minimum of nine faulting events involving the development of multiple surface ruptures, locally accompanied by folding in the unconsolidated Holocene deposits. The oldest recorded surface-rupturing event (event R), for which timing can be bracketed at 4290–4500 cal yr B.P., deformed colluvial unit 2 and created a scarp associated with fault F5 that led to the deposition of a 48-cm-thick colluvial wedge (unit 3). Unit 4, consisting of horizontally laminated fluvial sand with peat beds, suggests that subsidence at the foot of the scarp generated a poorly drained depression affected by periodic flooding. Considering that fault scarps tend to be about twice as high as the associated colluvial wedges (McCalpin, 2009b), we can roughly estimate that the fault scarp was around 1.0 m high.

The second event (event S) is recorded by deposition of the 77-cm-thick upper colluvial wedge between 3330 and 4340 cal yr B.P. This surface-rupturing event rejuvenated the scarp, leading to the colluvial deposition that locally and temporally interrupted the sedimentation of the fine-grained unit 4. Considering the thickness of the wedge, the displacement on F5 would be around 1.5 m.

The third event (event T) is recorded by the formation of the depression associated with the upper graben, in which the fine-grained unit 6 was deposited. The age of the base of unit 6 (2680–2640 cal yr B.P.), deposition of which started immediately after the creation of the sediment trap, can be considered as a good approximation for the timing of this event (ca. 2.7 ka). Probably, displacement on fault F10 generated an antislope scarp that confined deposition of unit 6 in the upper graben, as suggested by the absence of this unit in the downthrown block to the west of the horst. The thickness of unit 6 (81.5 cm), the top of which corresponds to an erosional contact, provides a minimum estimate for the vertical displacement achieved in this faulting event.

The fourth event (event U) occurred between 2340 and 2680 cal yr B.P. It is inferred from deformed units in the upper graben and the western downthrown block. In the upper graben, extension associated with fault F11 led to the formation of a fissure that is 42 cm wide. This fissure cuts through units 2 and 6 and is truncated by unit 7. The throw on fault F11 is just 17 cm. Moreover, on the eastern margin of the upper graben, unit 6 is offset by fault F12 with a minimum vertical displacement of 2.5 cm; unit 6 was eroded from the footwall. In the western downthrown block, this event is recorded by offset of units 2 and 4 on fault F1, which is truncated by unit 7. From the exposed thickness of unit 2 in the footwall, we can estimate a minimum throw of 45.1 cm on fault F1. The sum of the displacements yields a minimum total offset of around 65 cm for event U.

The structural and stratigraphic evidence of the fifth event (event V), which occurred between 2460 and 2340 cal yr B.P., includes in the downthrown block: (1) offset of unit 7 and older units by fault F2 with a vertical displacement of 50 cm, where fault F2 is truncated by unit 8; (2) faulting of units 4 and 7 and the two colluvial wedges (units 3 and 5) by fault F3 and F4 with a total vertical displacement of 3.5 cm; (3) development of a drag fold on both colluvial wedges (units 3 and 5) and units 4 and 7 due to slip on fault F5 (using the base of the upper colluvial wedge [unit 5], and assuming a horizontal original attitude, we estimate a minimum vertical displacement of 56 cm due to dragging along F5); and (4) disharmonic folding of units 4 and 7 related to local compression between faults F2 and F3. A minimum vertical cumulative displacement of 1.09 m is required to explain the deformational structures affecting these units, which are all truncated by unit 8.

The next three events (event W, X, and Y) took place in a short time span between 2140 and 2360 cal yr B.P. Unfortunately, it was impossible to better constrain their chronology. The sixth event (event W) is recorded by: (1) the offset of units 8 and 9 by faults F5 and F6 in the western downthrown block, with a minimum cumulative vertical throw of 32 cm since unit 8 has been eroded from the footwall of fault F6, and truncation of faults F5 and F6 by unit 10, which unconformably overlies the faulted unit 9; and (2) rotation of unit 9 by 7° to the west according to our retrodeformational analysis. Considering the dip of 2° in the western part of the half graben as the original angle of deposition, the vertical displacement required to restore unit 9 to its original orientation is 35 cm. Thus, the total displacement for this faulting event was over 67 cm.

The seventh event (event X) caused significant vertical displacement on fault F10 in the upper graben. The fault postdates unit 10 and precedes unit 11, which was deposited across the shear zone associated with fault

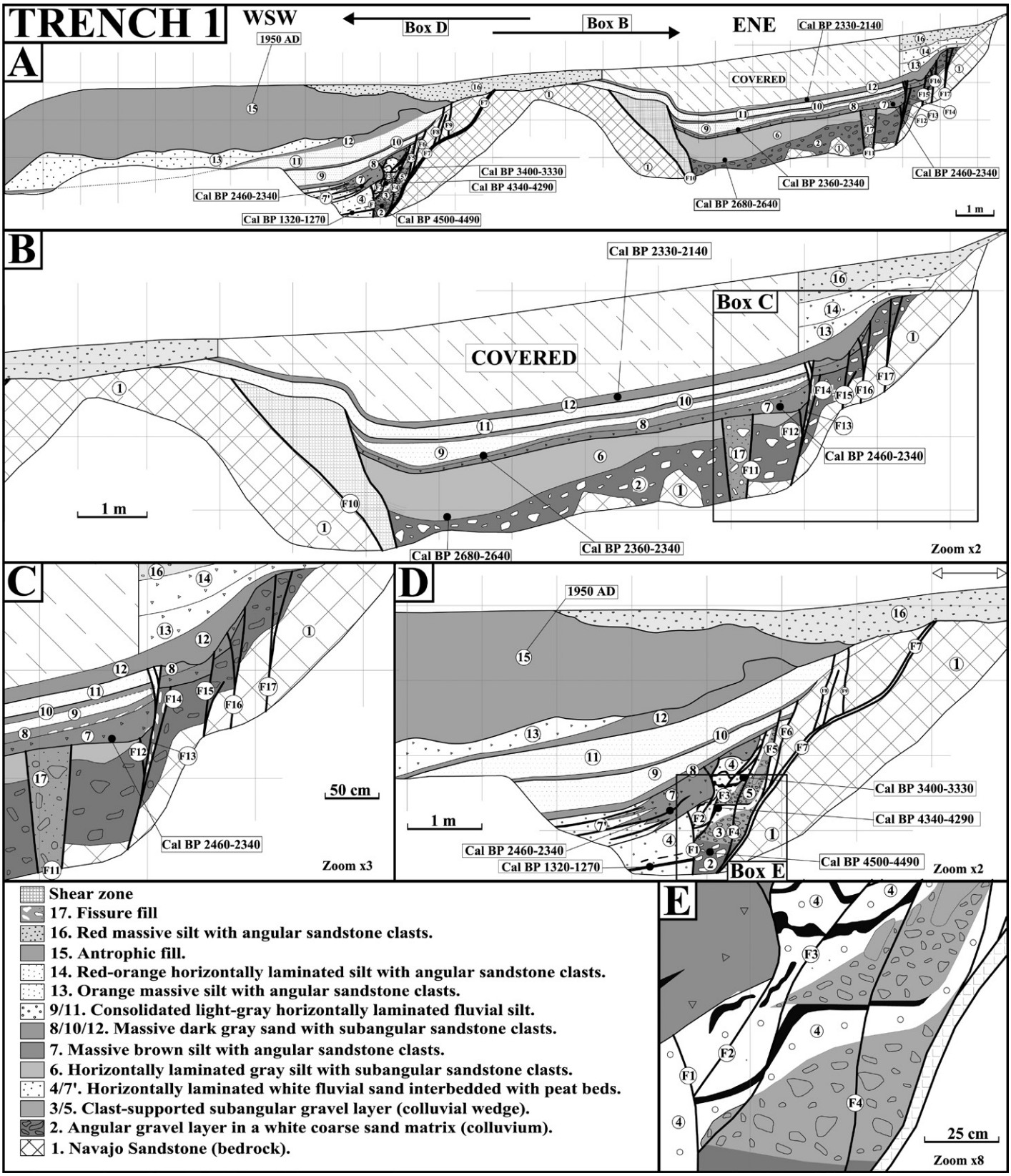

Figure 6. Log of trench 1 (A) and close-up areas (B–E). A more extensive description of units may be found in section 3 of the Data Repository (see text footnote 1).

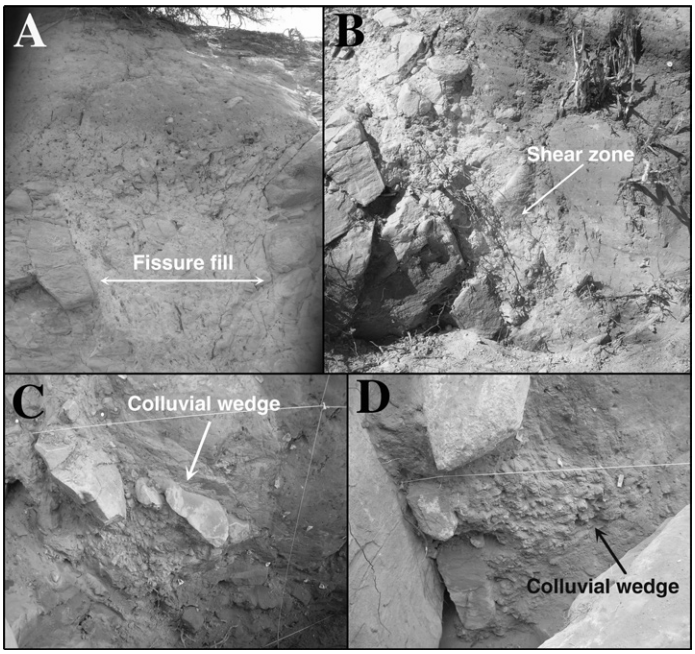

Figure 7. Deformation structures exposed in trench 1: (A) fissure fill located at the eastern margin of the upper graben in the SE wall of trench 1; (B) shear zone associated to fault F10 located at the southern margin of the upper graben in the NW wall of trench 1; and (C–D) upper and lower colluvial wedges associated with the margin of the downthrown block on the western sector of trench 1.

F10. Deposition of units 7–13 in the upper graben and western downthrown block suggests that the vertical displacement on fault F10 was not enough to restrict sedimentation in the upper graben. Therefore, the vertical distance between the base of unit 7 in the hanging wall and the top of the shear zone (unit 17) provides a minimum throw of at least 96 cm, since unit 7 has been eroded in the footwall of F10.

The eighth event (event Y) displaced units 7–11 in the upper graben by motion on faults F13, F15, and F16, all of which predate unit 12. These structures record a minimum cumulative throw of 1.13 m.

The most recent event, or MRE (event Z), occurred after 2330 cal yr B.P. and affected the youngest dated unit in both grabens (unit 12). In the upper graben, movement along faults F10, F16, and F17 was accommodated by ductile deformation and the development of monoclinal drape folds at both margins of the graben. In the western block, dragging along F7 tilted unit 13 and the underlying ones. Assuming a syndepositional dip of 2° for unit 12, which is the gradient of the lowest present-day slope, we measure a minimum net vertical displacement due to tilting of 2.36 m. Because 2.36 m is significantly greater than that of all previous events, it is possible that cumulative ductile deformation was caused by two or more events instead of just one faulting event.

Fault History

The slip history diagram (Fig. 8) shows seven closed and two open displacement cycles. The diagram has been constructed considering (1) the value of the age ranges assigned to single events; (2) uniform recurrence for the last three cycles, constrained by the same bracketing ages; and (3) the available data on displacement, either rough estimates based on colluvial wedge thickness (events R and S) or minimum vertical displacement values. The mean slip rates and recurrence intervals computed for the seven cycles are, respectively, from the oldest to the youngest, as follows: ~2.67 mm/yr and 560 yr, >1 mm/yr and 815 yr, >1.22 mm/yr and 530 yr, >12.1 mm/yr and 90 yr, >8.7 mm/yr and 73 yr, >13.1 mm/yr and 73 yr, and >15.5 mm/yr and 73 yr. Considering a minimum cumulative vertical displacement of 6.81 m and a time span of 2218 yr for the seven cycles, we obtain a minimum mean vertical slip rate of 3.07 mm/yr and an average recurrence of 316 yr. The apparent minimum slip rate and the apparent recurrence computed for all the open and closed cycles are 2.26 mm/yr and 500 yr, respectively. In this latter calculation, we consider the age of the oldest dated sedimentary unit and the minimum total displacement (10.17 m) recorded in the trench.

Unfortunately, the chronology of the last faulting event is poorly constrained by a maximum age (2330 cal yr B.P.), since the youngest sediments exposed in the trench largely correspond to anthropogenic deposits accumulated on a man-made excavation surface. Nevertheless, the slip history suggests that the inferred MRE, which shows an anomalously high vertical displacement (>2.36 m), may actually correspond to two or more surface-rupturing events, supporting recurrent fault motion during the last

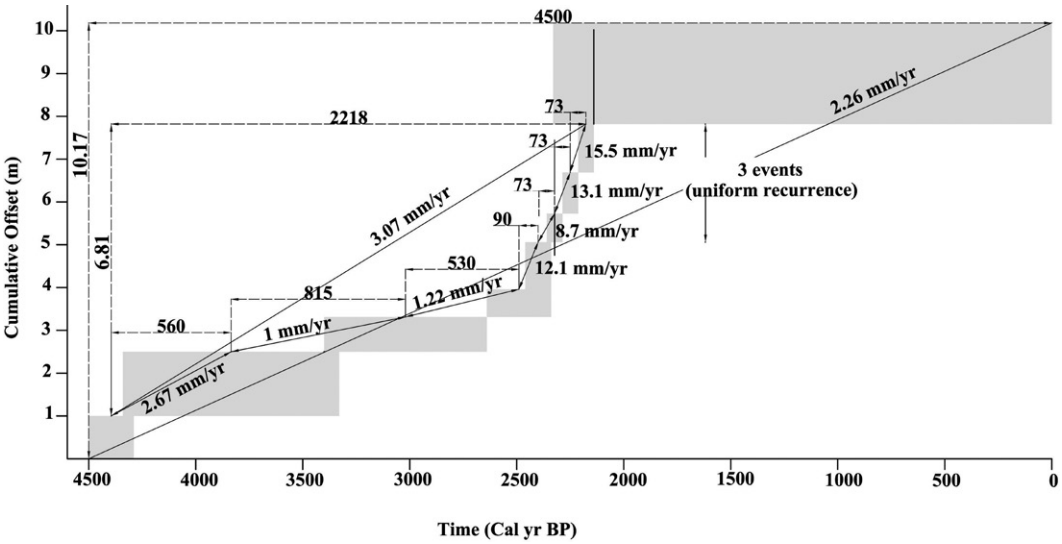

Figure 8. Slip history diagram of seven closed cycles showing the slip rate for each cycle and the seven cycles, as well as the apparent slip rate considering the age of the oldest dated sedimentary unit and cumulative vertical displacement. Most of the slip rates are derived from minimum displacement values and consequently correspond to minimum estimates. The gray areas represent the maximum length of every cycle incorporating 2σ uncertainties. A uniform recurrence is assumed for the last three displacement cycles, which are constrained by the same bracketing ages (2140–2360 cal yr B.P.).

two millennia. According to the hypothesis of two faulting events younger than 2330 cal yr B.P., the apparent average recurrence would be 450 yr or less. Regardless of the actual age of the last faulting event that occurred at the trench site, which most probably yields an underrepresented late Holocene deformation history, the available data strongly suggest that instantaneous dissolution-induced surface faulting is not an exhausted phenomenon in Spanish Valley. The existence of large subsidence depressions in the Colorado River floodplain (Fig. 1) provides geomorphic evidence of active evaporite dissolution and indicates that the karstic subsidence rate is notably higher than the local aggradation rates of the Colorado River and tributaries; otherwise, they would be quickly filled and obliterated by alluvial deposition. Moreover, the stacking of the Colorado River terraces in Spanish Valley as thickened alluvium (Smith and Goodknight, 2005) suggests that the Colorado River has been unable to keep pace with subsidence over a long period in the Quaternary. The regional incision rate of around 0.45 mm/yr estimated in the central Colorado Plateau over the late Pleistocene (Pederson et al., 2013a, 2103b) indicates a regional entrenchment trend that is clearly exceeded by the local base-level drop induced by salt-dissolution subsidence in Spanish Valley. The minimum slip rate of 3.07 mm/yr estimated in trench 1 for the main fault of the northeastern margin of the graben suggests that salt-dissolution subsidence may be locally six times greater than regional incision rates.

However, hydrochemical data from the Colorado River from 2003 to 2011 suggest limited salt dissolution in Spanish Valley at the present time (Shope and Gerner, 2014). According to Shope and Gerner, the salinity of the Colorado River between two measurement stations located 13 km upstream and 2 km downstream of Spanish Valley does not increase, showing a stable concentration of around 100 mg/L of chloride. According to Woodhouse et al. (2010) and U.S. Geological Survey (2004, 2011), the decrease in precipitation during the monitoring period might be responsible for a decline in groundwater recharge and the amount of evaporites dissolved. The significance of this observation is uncertain. That is, dissolution and hence subsidence and faulting in Spanish Valley may have ended permanently, but more likely, this hydrochemical evidence, based on a short record, may be of little significance to longer-term salt karstification processes, the episodic behavior of which might be closely related to climate variability.

SALT-DISSOLUTION VERSUS TECTONIC FAULTS

The stratigraphic and structural relationships observed in trenches 1 and 2 reveal episodic displacement on faults that accommodate subsidence caused by intrastratal dissolution of evaporites. Similar episodic faulting has been found in collapse sinkholes (Gutiérrez et al., 2009, 2011; Carbonel et al., 2014) and faults related to interstratal evaporite dissolution in Spain (Gutiérrez et al., 2012; Carbonel et al., 2013) and Colorado (Gutiérrez et al., 2014). Given that episodic faulting is the expected kinematic style for evaporite collapse structures, what other criteria may be robust discriminators of dissolution versus tectonic faulting? Here, we consider three fault parameters: (1) fault displacement to length ratio, (2) slip rate, and (3) statistical properties of the recurrence interval. Common scaling relationships for tectonic faults include ratios of maximum cumulative displacement to total fault length (D_{cum}/L), maximum coseismic displacement to total length (MD/L), average coseismic slip to fault length (AD/L), and average coseismic slip to maximum displacement (AD/MD). D_{cum}/L for tectonic faults with lengths similar to those in Spanish Valley show a broad range between 10^{-3} and 10^{-1} (Dawers et al., 1993; Schlische et al., 1996; Davis et al., 2005; Kim and Sanderson, 2005). We obtain a D_{cum}/L value of ~6×10^{-3} for the primary boundary fault along the northeastern margin of Spanish Valley, decreasing to 2×10^{-3} where trench 1 is located. The D_{cum}/L value calculated for the master synthetic fault of the marginal keystone graben is 9.6×10^{-3}. These ratios are comparable with those reported for extensional tectonic faults (Fig. 9).

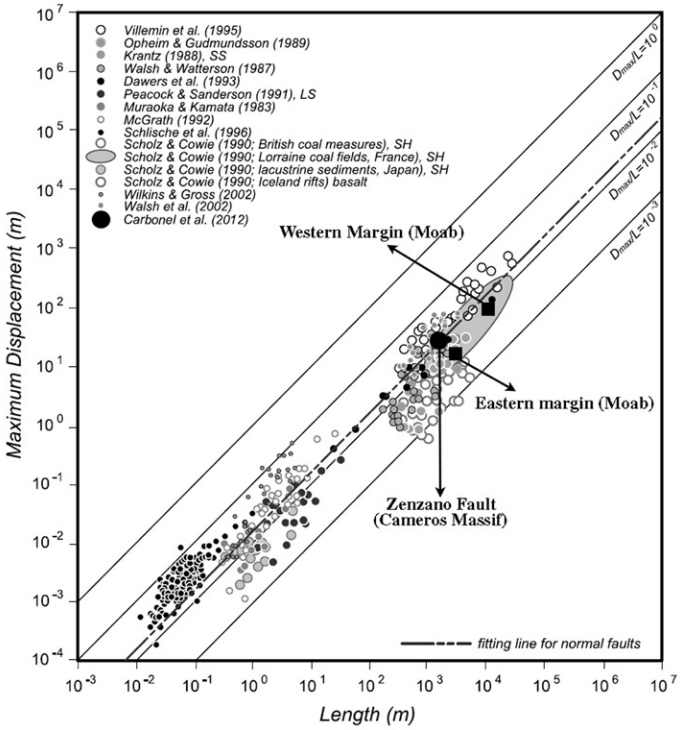

Figure 9. Log-log plot showing the maximum displacement against fault length of salt dissolution–induced faults in comparison with the data for tectonic faults presented by Kim and Sanderson (2005). SS—Sandstone; LS—Limestone; SH—Shale.

In contrast, the MD/L and AD/L ratios obtained for the salt dissolution–induced faults of Spanish Valley are significantly higher than those reported for tectonic faults (for extended explanation of slip-length ratio, see Shaw, 2013). Displacement measurements from trench 1 indicate a MD and an AD of 1.5 m and 1 m, respectively, for a fault around 5 km long. It is important to note that: (1) the inferred MD value corresponds to event S (the 2.36 m of displacement recorded in the MRE [event Z] was rejected from the analysis since it may be attributed to more than one faulting event, as discussed already), and (2) the AD is mainly derived from minimum values. Scholz (1994) pointed out that the MD/L ratio is usually on the order of 10^{-4}–10^{-5}. That is, the MD of a 5-km-long tectonic fault is expected to range between 50 cm and 5 cm. Similarly, the empirical relationships of Wells and Coppersmith (1994) and Leonard (2010) predict a maximum displacement per event (MD) of 6.7 cm and 20 cm. These values are 3–30, 20, and 7.5 times lower than the maximum displacement inferred in trench 1, respectively, for 5-km-long tectonic faults. Also according to those authors, an AD of 1 m would be expected for 30- and 36-km-long, normal fault surface ruptures, respectively. Regarding trench 2 (see section 4 of the Data Repository [see footnote 1]), the minimum MD and AD values estimated for the 350-m-long antithetic secondary normal fault investigated in trench 2 are 49 and 37 cm, respectively. The MD/L ratio is 14–140 times higher than Scholz's (1994) range. In addition, according to the relationships of Wells and Coppersmith (1994) and Leonard (2010), the obtained average slip would be expected from

surface-rupture lengths of 17 km and 11 km, respectively. Liu-Zeng et al. (2005) suggested that the AD/L ratio fits a linear relationship given by the formula $D = (2.5 \times 10^{-5})L$ (Fig. 10). The AD values of trench 1 and trench 2 are 8 and 42 times higher than the expected values for tectonic faults using the formula of Liu-Zeng et al. (2005), respectively.

McCalpin (2009c), based on an extensive bibliographic review, indicated that the AD/MD ratio of tectonic faults averages around 0.5, with a range of 0.2–0.8. The AD/MD ratios calculated for the faults investigated in trenches 1 and 2 are 0.6 and 0.75, respectively, which seem to match with those reported for tectonic faults.

Slip rate and recurrence intervals may also be useful discriminators when classifying faults as tectonic versus nontectonic structures associated with evaporite dissolution. The fault exposed in trench 1 has a surprisingly high slip rate of >3.07 mm/yr calculated from seven closed slip cycles. These values are significantly greater than the slip rates for most tectonic normal faults. For example, the slip rate of the Wasatch fault along the eastern boundary of the Basin and Range Province in Utah ranges from 1.4 mm/yr to 0.12 mm/yr, depending on the segment and the time period over which slip is measured (Machette et al., 1992; McCalpin and Nishenko, 1996; Mattson and Bruhn, 2001; Friedrich et al., 2003; Lund, 2005; Chang et al., 2006; Mayo et al., 2009). The average slip rate at Spanish Valley is between 2 and 25 times greater than the range estimated for the Wasatch fault.

The slip history diagram derived from trench 1 shows stochastic behavior with a large variation in the closed cycle average slip rates and average recurrences, with ranges of 1–15 mm/yr and 815–73 yr, respectively (Fig. 8). The coefficient of variation (CV) or aperiodicity (standard deviation of the recurrence data/long-term average earthquake recurrence), which simply reflects the variability in the recurrence interval, is 1.04. In extensional tectonic settings, there is an increasing body of evidence indicating that slip rate and recurrence vary in space and time (Mitchell et al., 2001; Friedrich et al., 2003; Bull et al., 2006; Nicol et al., 2009). Values of CV quoted in the literature vary from 0.02 to 1.0 (Ellsworth et al., 1999; Cowie et al., 2012), approaching a more representative value of 0.3–0.5 as the number of dated paleoearthquake ruptures increases, to provide a more complete fault rupture history (Console et al., 2008; McCalpin, 2009c; Schlagenhauf et al., 2010). The obtained CV value of 1.04 is around double that expected for a tectonic fault.

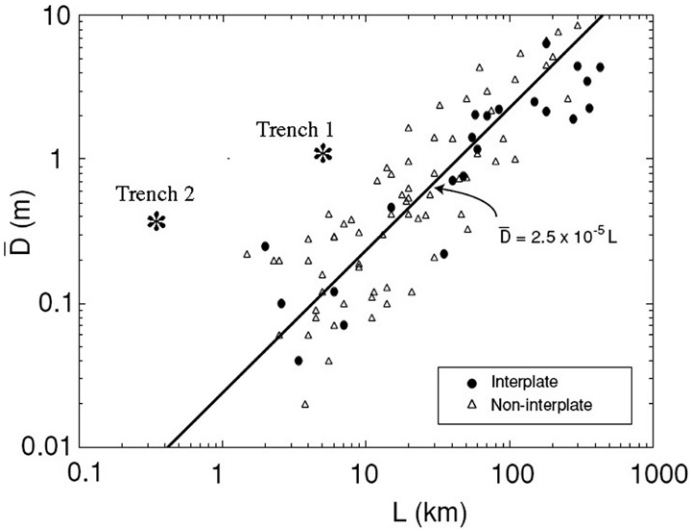

Figure 10. Slip-length relation of Moab salt dissolution–induced faults in comparison with interplate (circles) and non-interplate (triangles) tectonic earthquakes presented by Liu-Zeng et al. (2005) in a log-log plot.

CONCLUSIONS

The karstic subsidence of the crest of the Spanish Valley salt-intruded anticline has led to the folding and collapse of the overlying strata, which have been buried by a stepped sequence of six terrace levels and four covered pediment levels correlative to some of the terraces at the bottom of the valley. The anomalies of the longitudinal profile of the older terraces at the southern end of the valley together with the existence of a complex pattern of buried soils beneath the planar depositional surface of terrace T3 support Harden et al.'s (1985) studies that older terraces converge downstream to form a single thickened alluvial surface made up of superimposed terrace fills in the graben.

The extension related to the intrastratal dissolution of the Paradox Formation has produced a sequence of anticlines and synclines that are 50–400 m in wavelength and up to 17 km long, trending NW-SE parallel to the axis of the graben on both margins of the valley. The limb and hinge of the folds are often affected by swarms of synthetic and antithetic normal faults, giving rise to an intensely brecciated stratigraphic sequence with highly variable strikes and dips. The gravitational deformation attenuates toward the southeastern end of the valley, where the number of normal faults and the dip of the fold limbs gradually decrease to form single monoclines with dips in the limbs of 20°–30° on both flanks of the valley. This complex deformational context fits well with Gutiérrez's (2004) interstratal karstification model of salt anticlines.

A trench, 27 m long and 4.5 m deep, was excavated across the hanging wall of the 5-km-long primary normal fault of the eastern flank. The trench shows a complex structure made up of an upper graben and a lower half graben separated by a horst structure. The structural and stratigraphic relationships observed in the trench may be explained by a minimum of nine faulting events involving the development of multiple surface ruptures, the flexure and ductile deformation of units, and the formation of a fissure fill and two colluvial wedges, which are interpreted as evidences of episodic displacement. The slip history diagram of the fault shows seven closed and two open seismic cycles that allow us to obtain the following parameters: (1) D_{cum}/Length ratio of 6×10^{-3} in the middle sector and 2×10^{-3} where trench 1 was located, close to the SE edge of the mapped trace of the fault, values which are similar to those expected from tectonic faults; (2) from 2 to 25 times higher slip rate than the Wasatch fault, with an average slip rate of 3.07 mm/yr and an average recurrence interval of 316 yr calculated from seven closed slip cycles; (3) a stochastic regime with a CV value of 1.04, which is double that of tectonic faults with a long paleoseismologic record; (4) a maximum displacement (MD) of 1.5 m, which is 3–30 times higher than tectonic faults of the same length; and (5) an average slip displacement (AD) of 1 m. This value is 5–15 times higher than the expected AD for a 5-km-long tectonic fault according to the empirical relationships of Wells and Coppersmith (1994) and Leonard (2010).

Salt dissolution–induced faults show an episodic behavior but do not follow the experimental relationships used to characterized normal seismogenic tectonic faults. Although both types of faults have similar aspect ratios, salt-dissolution faults will probably yield: (1) higher long-term slip rates than the surrounding tectonic faults because the rate of salt dissolution will probably be higher than the telluric movement rate, (2) a random behavior with very high CV values, probably due to changes in the dissolution rate and karstic hydrogeological system, and (3) a very high slip per event in relation to their length. These differences would allow the genesis of faults in complex areas affected by tectonic activity and salt dissolution to be distinguished and the possible seismic risk related to them to be determined.

ACKNOWLEDGMENTS

The work has been partially financed by the projects CGL2010-16775 (Ministerio de Ciencia e Innovación and FEDER) and CGL2013-40867-P (Ministerio de Economía y Competitividad). Jesús Guerrero carried out a postdoctoral stay at the University of Utah funded by the Ministerio de Educación of Spain. The authors acknowledge the assistance provided by Helmut Doelling. Thanks go to the City Hall of Moab, for approving a permit to work on the artificial excavation corresponding to trench 1.

REFERENCES CITED

Alkattan, M., Oelkers, E.H., Dandurand, J.L., and Schott, J., 1997, Experimental studies of halite dissolution kinetics. The effect of saturation state and the presence of trace metals: Chemical Geology, v. 137, p. 201–219, doi:10.1016/S0009-2541(96)00164-7.

Baars, D.L., and Doelling, H.H., 1987, Moab salt-intruded anticline, east-central Utah: Boulder, Colorado, Rocky Mountain Section, Geological Society of America Centennial Field Guide, p. 275–280.

Baars, D.L., and Stevenson, G.M., 1981, Tectonic evolution of the Paradox Basin, Utah and Colorado, *in* Wiegand, D.L., ed., Geology of the Paradox Basin: Denver, Colorado, Rocky Mountain Association of Geologists, p. 23–31.

Barbeau, D.L., 2003, A flexural model for the Paradox Basin: Implications for the tectonics of the ancestral Rocky Mountains: Basin Research, v. 15, p. 97–115, doi:10.1046/j.1365-2117.2003.00194.x.

Berg, S.S., and Skar, T., 2005, Controls on damage zone asymmetry of a normal fault zone: Outcrop analyses of a segment of the Moab fault, SE Utah: Journal of Structural Geology, v. 27, p. 1803–1822, doi:10.1016/j.jsg.2005.04.012.

Berner, R.A., 1978, Rate control of mineral dissolution under earth surface conditions: American Journal of Science, v. 278, p. 1235–1252, doi:10.2475/ajs.278.9.1235.

Biggar, N.E., Harden, D.R., and Gillan, M.L., 1981, Quaternary deposits in the Paradox Basin, *in* Wiegand, D.L., ed., Geology of the Paradox Basin: Denver, Colorado, Rocky Mountain Association of Geologists, p. 129–143.

Birk, S., Liedl, R., Sauter, M., and Teutsch, G., 2003, Hydraulic boundary conditions as a controlling factor in karst genesis: A numerical modelling study on artesian conduit development in gypsum: Water Resources Research, v. 39, no. 1, p. SBH1-1–SBH1-13, doi:10.1029/2002WR001308.

Blount, C.W., and Dickson, F.W., 1973, Gypsum-anhydrite equilibria in systems $CaSO_4$-H_2O and $CaCO_3$-NaCl-H_2O: The American Mineralogist, v. 58, p. 323–331.

Bull, J.M., Barnes, P.M., Lamarche, G., Sanderson, D.J., Cowie, P.A., Taylor, S.K., and Dix, J.K., 2006, High-resolution record of displacement accumulation on an active normal fault: Implications for models of slip accumulation during repeated earthquakes: Journal of Structural Geology, v. 28, p. 1146–1166, doi:10.1016/j.jsg.2006.03.006.

Carbonel, D., Gutiérrez, F., Linares, R., Roqué, C., Zarroca, M., McCalpin, J., Guerrero, J., and Rodríguez, V., 2013, Differentiating between gravitational and tectonic faults by means of geomorphological mapping, trenching and geophysical surveys: The case of the Zenzano fault (Iberian Chain, N Spain): Geomorphology, v. 189, p. 93–108, doi:10.1016/j.geomorph.2013.01.020.

Carbonel, D., Rodríguez, V., Gutiérrez, F., McCalpin, J.P., Linares, R., Roqué, C., Zarroca, M., and Guerrero, J., 2014, Sinkhole characterisation combining trenching, ground penetrating radar (GPR) and electrical resistivity tomography (ERT): Earth Surface Processes and Landforms, v. 39, p. 214–227, doi:10.1002/esp.3440.

Cater, F., 1970, Geology of the Salt Anticline Region in Southwestern Colorado: U.S. Geological Survey Professional Paper 637, 80 p.

Chang, W.-L., Smith, R.B., Meertens, C.M., and Harris, R.A., 2006, Contemporary deformation of the Wasatch fault, Utah, from GPS measurements with implications for interseismic fault behavior and earthquake hazard: Observations with kinematic analysis: Journal of Geophysical Research, v. 111, no. B11, B11405, doi:10.1029/2006JB004326.

Console, R., Murru, M., Falcone, G., and Catalli, F., 2008, Stress interaction effect on the occurrence probability of characteristic earthquakes in the central Apennines: Journal of Geophysical Research, v. 113, p. B08313, doi:10.1029/2007JB005418.

Cowie, P.A., Roberts, G.P., Bull, J.M., and Visini, F., 2012, Relationships between fault geometry, slip rate variability and earthquake recurrence in extensional settings: Geophysical Journal International, v. 189, p. 143–160, doi:10.1111/j.1365-246X.2012.05378.x.

Dahm, T., Heimann, S., and Bialowons, W., 2011, A seismological study of shallow weak microearthquakes in the urban area of Hamburg city, Germany, and its possible relation to salt dissolution: Natural Hazards, v. 58, p. 1111–1134, doi:10.1007/s11069-011-9716-9.

Davis, K., Burbank, D.W., Fisher, D., Wallace, S., and Nobes, D., 2005, Thrust-fault growth and segment linkage in the active Ostler fault zone, New Zealand: Journal of Structural Geology, v. 27, p. 1528–1546, doi:10.1016/j.jsg.2005.04.011.

Dawers, N.H., Anders, M.H., and Scholz, C.H., 1993, Growth of normal faults: Displacement-length scaling: Geology, v. 21, p. 1107–1110, doi:10.1130/0091-7613(1993)021<1107:GONFDL>2.3.CO;2.

Doelling, H.H., 1988, Geology of Salt Valley anticline and Arches National Park, Grand County, Utah, *in* Doelling, H.H., Oviatt, C.G., and Huntoon, P.W., eds., Salt Deformation in the Paradox Region: Utah Geological and Mineral Survey Bulletin 122, p. 7–58.

Doelling, H.H., 2000, Geology of Arches National Park, Grand County, Utah, *in* Sprinkel, D.A., Chidsey, T.C., and Anderson, P.B., eds., Geology of Utah's Parks and Monuments: Utah Geological Association Publication 28, p. 11–36.

Doelling, H.H., 2001, Geologic Map of the Moab and Eastern Part of the San Rafael Desert 30′ × 60′ Quadrangles, Grand and Emery Counties, Utah, and Mesa County, Colorado: Utah Geological Survey Map 180, scale 1:100,000, 3 sheets.

Doelling, H.H., 2004, Geologic Map of the La Sal 30′ × 60′ Quadrangle, San Juan, Wayne and Garfield Counties, Utah, and Montrose and San Miguel Counties, Colorado: Utah Geological Survey Map 205, scale 1:100,000, 3 sheets.

Doelling, H.H., Ross, M.L., and Mulvey, M.L., 2002, Geologic Map of the Moab 7.5′ Quadrangle, Grand County, Utah: Utah Geological Survey Map 181, scale 1:24,000, 2 sheets.

Dove, P.M., and Czank, C.A., 1995, Crystal chemical controls on the dissolution kinetics of the isostructural sulfates: Celestite, anglesite and barite: Geochimica et Cosmochimica Acta, v. 59, p. 1907–1915, doi:10.1016/0016-7037(95)00116-6.

Ellsworth, W.L., Matthews, M.V., Nadeau, R.M., Nishenko, S.P., Reasenberg, P.A., and Simpson, R.W., 1999, A Physically-Based Earthquake Recurrence model for Estimation of Long-Term Earthquake Probabilities: U.S. Geological Survey Open-File Report 522, 22 p.

Ewers, R.O., 1982, Cavern Development in the Dimensions of Length and Breadth [Ph.D. thesis]: Ontario, McMaster University, Hamilton, 398 p.

Ewers, R.O., and Quinlan, J.F., 1981, Cavern porosity development in limestone: A low dip model from Mammoth Cave, *in* Beck, B., ed., Proceedings of the 8th International Congress of Speleology: Bowling Green, Ohio, Americus, p. 721–731.

Ford, D., and Williams, P., 1989, Karst Geomorphology and Hydrology: Winchester, Massachusetts, Unwin Hyman, 320 p.

Foxford, K.A., Garden, I.R., Guscott, S.C., Burley, S.D., Lewis, J.J.M., Walsh, J.J., and Watterson, J., 1996, The field geology of the Moab fault, *in* Huffman, A.C., Jr., Lund, W.R., and Goodwin, L.H., eds., Geology and Resources of the Paradox Basin Utah: Salt Lake City Geological Association Guidebook 25, p. 265–283.

Freyer, D., and Voigt, W., 2004, The measurement of sulfate mineral solubilities in the Na-K-Ca-Cl-SO_4-H_2O system at temperatures of 100, 150 and 200°C: Geochimica et Cosmochimica Acta, v. 68, p. 307–318, doi:10.1016/S0016-7037(03)00215-1.

Friedrich, A.M., Wernicke, B.P., Niemi, N.A., Bennett, R.A., and Davis, J.L., 2003, Comparison of geodetic and geologic data from the Wasatch region, Utah, and implications for the spectral character of Earth deformation at periods of 10 to 10 million years: Journal of Geophysical Research, v. 108, no. B4, p. 2199, doi:10.1029/2001JB000682.

Garden, R., Guscott, S.C., Burley, S.D., Foxford, K.A., Walsh, J.J., and Marshall, J., 2001, An exhumed palaeo-hydrocarbon migration fairway in a faulted carrier system, Entrada Sandstone of SE Utah, USA: Geofluids, v. 1, p. 195–213, doi:10.1046/j.1468-8123.2001.00018.x.

Guerrero, J., Gutiérrez, F., and Lucha, P., 2008, The impact of halite dissolution subsidence on fluvial terrace development. The case study of the Huerva River in the Ebro Basin (NE Spain): Geomorphology, v. 100, p. 164–179, doi:10.1016/j.geomorph.2007.04.040.

Gutiérrez, F., 2004, Origin of the salt valleys in the Canyonlands section of the Colorado Plateau: Evaporite-dissolution collapse versus tectonic subsidence: Geomorphology, v. 57, p. 423–435, doi:10.1016/S0169-555X(03)00186-7.

Gutiérrez, F., Guerrero, J., and Lucha, P., 2008, A genetic classification of sinkholes illustrated from evaporite paleokarst exposures in Spain: Environmental Geology, v. 53, p. 993–1006, doi:10.1007/s00254-007-0727-5.

Gutiérrez, F., Galve, J.P., Lucha, P., Bonachea, J., Jordá, L., and Jordá, R., 2009, Investigation of a large collapse sinkhole affecting a multi-storey building by means of geophysics and the trenching technique, Zaragoza City, NE Spain: Environmental Geology, v. 58, p. 1107–1122, doi:10.1007/s00254-008-1590-8.

Gutiérrez, F., Galve, J.P., Lucha, P., Castañeda, C., Bonachea, J., and Guerrero, J., 2011, Integrating geomorphological mapping, trenching, InSAR and GPR for the identification and characterization of sinkholes in the mantled evaporite karst of the Ebro Valley (NE Spain): Geomorphology, v. 134, p. 144–156, doi:10.1016/j.geomorph.2011.01.018.

Gutiérrez, F., Carbonel, D., Guerrero, J., McCalpin, J.P., Linares, R., Roque, C., and Zarroca, M., 2012, Late Holocene episodic displacement on fault scarps related to interstratal dissolution of evaporites (Teruel Neogene Graben, NE Spain): Journal of Structural Geology, v. 34, p. 2–19, doi:10.1016/j.jsg.2011.11.006.

Gutiérrez, F., Carbonel, D., Kirkham, R.M., Guerrero, J., Lucha, P., and Matthews, V., 2014, Can flexural-slip faults related to evaporite dissolution generate hazardous earthquakes? The case of the Grand Hogback monocline of west-central Colorado: Geological Society of America Bulletin, published online, doi:10.1130/B31054.1.

Harden, D.R., Biggar, N.E., and Guillan, M.L., 1985, Quaternary deposits and soils in and around Spanish Valley, Utah, *in* Weide, D.L., ed., Soils and Quaternary Geology of the Southwestern United States: Geological Society of America Special Paper 203, p. 43–64.

Hite, R.J., 1960, Stratigraphy of the saline facies of the Paradox member of the Hermosa Formation, *in* Smith, K.G., ed., Geology of the Paradox Basin Fold and Fault Belt, Third Field Conference Guidebook: Durango, Colorado, Four Corners Geological Society, p. 86–89.

Hoffman, M., Stockli, D., Kelley, S.A., Pederson, J., and Lee, J., 2011, Mio-Pliocene erosional exhumation of the central Colorado Plateau, eastern Utah: New insights from apatite (U-Th)/He thermochronometry, *in* Beard, L.S., Karlstrom, K.E., Young, R.E., and Billingsley, G.H., eds., CREvolution 2—Origin and Evolution of the Colorado River System: U.S. Geological Survey Open-File Report 2011-1210, Workshop Abstracts, p. 132–136.

Huntoon, P.W., 1999, Field-based identification of salt-related structures and their differentiation from tectonic structures, *in* Hanson, K.L., Kelson, K.I., Angell, M.A., and Lettis, W.R., eds., Techniques for Identifying Faults and Determining their Origins: Washington, D.C., U.S. Nuclear Regulatory Commission, contract report NUREG/CR-5503, 186 p. plus appendices.

Jeschke, A.A., Vosbeck, K., and Dreybrodt, W., 2001, Surface controlled dissolution rates of gypsum in aqueous solutions exhibit nonlinear dissolution kinetics: Geochimica et Cosmochimica Acta, v. 65, p. 27–34, doi:10.1016/S0016-7037(00)00510-X.

Jousset, P., and Rohmer, J., 2012, Evidence for remotely triggered microearthquakes during salt cavern collapse: Geophysical Journal International, v. 191, p. 207–223, doi:10.1111/j.1365-246X.2012.05598.x.

Kim, Y., and Sanderson, D.J., 2005, The relationship between displacement and length of faults, a review: Earth-Science Reviews, v. 68, p. 317–334, doi:10.1016/j.earscirev.2004.06.003.

Krantz, R.W., 1988, Multiple fault sets and three-dimensional strain: Journal of Structural Geology, v. 10, p. 225–237, doi:10.1016/0191-8141(88)90056-9.

Land, L., 2013, Geophysical records of anthropogenic sinkhole formation in the Delaware Basin region, southeast New Mexico and west Texas, USA: Carbonates and Evaporites, v. 28, no. 1–2, p. 183–190, doi:10.1007/s13146-013-0126-9.

Lauritzen, S.E., and Lundberg, J., 2000, Solutional and erosional morphology, *in* Klimchouk, A., Ford, D., Palmer, A., and Dreybrodt, W., eds., Speleogenesis Evolution of Karst Aquifers: Huntsville, Alabama, National Speleological Society, p. 408–426.

Lenti, L., Martino, S., Paciello, A., Prestininzi, A., and Rivellino, S., 2012, Microseismicity within a karstified rock mass due to cracks and collapses as a tool for risk management: Natural Hazards, v. 64, p. 359–379, doi:10.1007/s11069-012-0245-y.

Leonard, M., 2010, Earthquake fault scaling: Self-consistent relating of rupture length, width, average displacement, and moment release: Bulletin of the Seismological Society of America, v. 100, p. 1971–1988, doi:10.1785/0120090189.

Liu-Zeng, J., Heaton, T., and DiCaprio, C., 2005, The effect of slip variability on earthquake slip-length scaling: Geophysical Journal International, v. 162, p. 841–849, doi:10.1111/j.1365-246X.2005.02679.x.

Lund, W.R., 2005, Consensus Preferred Recurrence-Interval and Vertical Slip-Rate Estimates: Review of Utah Paleoseismic-Trenching Data by the Utah Quaternary Fault Parameters Working Group: Utah Geological Survey Bulletin 134, 26 p.

Machette, M.N., Personius, S.F., and Nelson, A.R., 1992, Paleoseismology of the Wasatch fault zone: A summary of recent investigations, conclusions, and interpretations, *in* Gory, P.L., and Hays, W.W. eds., Assessment of Regional Earthquake Hazards and Risk along the Wasatch Front: U.S. Geological Survey Professional Paper 1500, p. A1–A72.

Mattson, A., and Bruhn, R.L., 2001, Fault slip rate and initiation age based on diffusion equation modeling: Wasatch fault zone and eastern Great Basin: Journal of Geophysical Research, v. 106, no. B7, p. 13,739–13,750, doi:10.1029/2001JB900003.

Mayo, A.L., Bruthans, J., Tingey, D., Kadlec, J., and Nelson, S., 2009, Insights into Wasatch fault vertical slip rates using the age of sediments in Timpanogos Cave: Utah: Quaternary Research, v. 72, p. 275–283, doi:10.1016/j.yqres.2009.04.006.

McCalpin, J.P., 2009a, Field techniques in paleoseismology-terrestrial environments, *in* McCalpin, J.P., ed., Paleoseismology (2nd ed.): San Diego, California, Academic Press, p. 29–117.

McCalpin, J.P., 2009b, Paleoseismology in extensional tectonic environments, *in* McCalpin, J.P., ed., Paleoseismology (2nd ed.): San Diego, California, Academic Press, p. 171–277.

McCalpin, J.P., 2009c, Application of paleoseismic data to SHA and neotectonic research, *in* McCalpin, J.P., ed., Paleoseismology (2nd ed.): San Diego, California, Academic Press, chapter 9, p. 1–101.

McCalpin, J.P., and Nishenko, S.P., 1996, Holocene paleoseismicity, temporal clustering, and probabilities of future large (M >7) earthquakes on the Wasatch fault zone, Utah: Journal of Geophysical Research, v. 101, no. B3, p. 6233–6253, doi:10.1029/95JB02851.

McGrath, A., 1992, Fault propagation and growth. A study of the Triassic and Jurassic from Watchet and Kilve, North Somerset [M.S. thesis]: London, Royal Holloway, University of London, 165 p.

McMurry, J., 2004, Chemistry (4th ed.): New York, Prentice-Hall, Inc., 1328 p.

Mitchell, S.G., Matmon, A., Bierman, P.R., Enzel, Y., Caffee, M., and Rizzo, D., 2001, Displacement history of a limestone normal fault scarp, northern Israel, from cosmogenic ^{36}Cl: Journal of Geophysical Research, v. 106, p. 4247–4264, doi:10.1029/2000JB900373.

Muraoka, H., and Kamata, H., 1983, Displacement distribution along minor fault traces: Journal of Structural Geology, v. 5, p. 483–495, doi:10.1016/0191-8141(83)90054-8.

Newton, R.C., and Manning, C.E., 2005, Solubility of anhydrite, $CaSO_4$ in NaCl-H_2O solutions at high pressures and temperatures, applications to fluid-rock interaction: Journal of Petrology, v. 46, p. 701–716, doi:10.1093/petrology/egh094.

Nicol, A., Walsh, J., Mouslopoulou, V., and Villamor, P., 2009, Earthquake histories and Holocene acceleration in fault displacement rates: Geology, v. 37, p. 911–914, doi:10.1130/G25765A.1.

Olig, S.S., Fenton, C.H., McCleary, J., and Wong, I.G., 1996, The earthquake potential of the Moab fault and its relation to salt tectonics in the Paradox Basin, Utah, *in* Huffman, A.C., Jr., Lund, W.R., and Goodwin, L.H., eds., Geology and Resources of the Paradox Basin: Utah Geological Association Guidebook 25, p. 251–264.

Opheim, J.A., and Gudmundsson, A., 1989, Formation and geometry of fractures, and related volcanism, of the Krafla fissure swarm, northeast Iceland: Geological Society of America Bulletin, v. 101, p. 1608–1622, doi:10.1130/0016-7606(1989)101<1608:FAGOFA>2.3.CO;2.

Palmer, A.N., 2000, Hydrogeologic control of cave patterns, *in* Klimchouk, A., Ford, D., Palmer, A., and Dreybrodt, W., eds., Speleogenesis Evolution of Karst Aquifers: Huntsville, Alabama, National Speleological Society, p. 77–90.

Peacock, D.C.P., and Sanderson, D.J., 1991, Displacement and segment linkage and relay ramps in normal fault zones: Journal of Structural Geology, v. 13, p. 721–733, doi:10.1016/0191-8141(91)90033-F.

Pederson, J., Cragun, W.S., Hidy, A.J., Rittenour, T.M., and Gosse, J.C., 2013a, Colorado River chronostratigraphy at Lee's Ferry, Arizona, and the central Colorado Plateau bull's-eye of incision: Geology, v. 41, p. 427–430, doi:10.1130/G34051.1.

Pederson, J., Burnside, N., Shipton, Z., and Rittenour, T., 2013b, Rapid river incision across an inactive fault: Implications for patterns of erosion and deformation in the central Colorado Plateau: Lithosphere, v. 5, no. 5, p. 513–520, doi:10.1130/L282.1.

Pevear, D.R., Vrolijk, P.J., and Longstaffe, F.J., 1997, Timing of Moab fault displacement and fluid movement integrated with burial history using radiogenic and stable isotopes, *in* Hendry, J., Carey, P., Parnell, J., Ruffell, A., and Worden, R., eds., Geofluids II '97: Contributions to the Second International Conference on Fluid Evolution, Migration and Interaction in Sedimentary Basins and Orogenic Belts: Belfast, The Queen's University, p. 42–45.

Ponsjack, E., 1940, Deposition of calcium sulphate from sea water: American Journal of Science, v. 239, p. 559–568.

Raines, M.A., and Dewers, T.A., 1997, Mixed-transport/reaction control of gypsum dissolution kinetics in aqueous solutions and initiation of gypsum karst: Chemical Geology, v. 140, p. 29–48, doi:10.1016/S0009-2541(97)00018-1.

Reimer, P.J., Baillie, M.G.L., Bard, E., Bayliss, A., Beck, J.W., Bertrand, C.J.H., Blackwell, P.G., Buck, C.E., Burr, G.S., Cutler, K.B., Damon, P.E., Edwards, R.L., Fairbanks, R.G., Friedrich, M., Guilderson, T.P., Hogg, A.G., Hughen, K.A., Kromer, B., McCormac, G., Manning, S., Bronk, R.C., Reimer, R.W., Remmele, S., Southon, J.R., Stuiver, M., Talamo, S., Taylor, F.W., Plicht, J., and Weyhenmeyer, C., 2004, IntCal04: Terrestrial radiocarbon age calibration, 0–26 Cal kyr BP: Radiocarbon, v. 46, no. 3, p. 1029–1058.

Schlagenhauf, A., Gaudemer, Y., Benedetti, L., Manighetti, I., Palumbo, L., Schimmelpfennig, I., Finkel, R., and Pou, K., 2010, Using in situ chlorine-36 cosmonuclide to recover past earthquake histories on limestone normal fault scarps: A reappraisal of methodology and interpretations: Geophysical Journal International, v. 182, p. 36–72.

Schlische, R.W., Young, S.S., Ackermann, R.V., and Gupta, A., 1996, Geometry and scaling relations of a population of very small rift-related normal faults: Geology, v. 24, p. 683–686, doi:10.1130/0091-7613(1996)024<0683:GASROA>2.3.CO;2.

Scholz, C.H., 1994, A reappraisal of large earthquake scaling: Bulletin of the Seismological Society of America, v. 84, p. 215–218.

Scholz, C.H., and Cowie, P.A., 1990, Determination of geologic strain from fault slip data: Nature, v. 346, p. 837–839, doi:10.1038/346837a0.

Shaw, B.E., 2013, Earthquake surface slip-length data is fit by constant stress drop and is useful for seismic hazard analysis: Bulletin of the Seismological Society of America, v. 103, p. 876–893, doi:10.1785/0120110258.

Shope, C.L., and Gerner, S.J., 2014, Assessment of Dissolved-Solids Loading to the Colorado River in the Paradox Basin between the Dolores River and Gypsum Canyon, Utah by the U.S. Bureau of Reclamation and the Colorado River Basin Salinity Control Forum: U.S. Geological Survey Scientific Investigations Report 2014-5031, 28 p.

Smith, G.M., and Goodknight, C.S., 2005, Quaternary salt dissolution in the Moab-Spanish Valley, UT, Pleistocene and Holocene evidence: Geological Society of America Abstracts with Programs, v. 37, no. 6, p. 6.

Solum, J.G., Van der Pluijm, B.A., and Peacor, D.R., 2005, Neocrystallization, fabrics and age of clay minerals from an exposure of the Moab fault, Utah: Journal of Structural Geology, v. 27, p. 1563–1576, doi:10.1016/j.jsg.2005.05.002.

Stevenson, G.M., and Baars, D.L., 1986, The Paradox, a pull-apart basin of Pennsylvanian age, *in* Peterson, J.A., ed., Paleotectonics and Sedimentation in the Rocky Mountain Region, United States: American Association of Petroleum Geology Memoir 41, p. 513–539.

Styles, P., 2003, Feature: Environmental geophysics: A site characterization tool for urban regeneration in the post-mining era: Geology Today, v. 19, p. 173–178, doi:10.1046/j.1365-2451.2003.00407.x.

Trifu, C., and Shumila, V., 2010, Microseismic monitoring of a controlled collapse in field II at Ocnele Mari, Romania: Pure and Applied Geophysics, v. 167, p. 27–42, doi:10.1007/s00024-009-0013-4.

U.S. Geological Survey, 2004, Climatic Fluctuations, Drought and Flow in the Colorado River Basin: U.S. Geological Survey Fact Sheet 2004-3062, version 2, 4 p.

U.S. Geological Survey, 2011, Quality of Water in the Colorado River Basin: Bureau of Reclamation Progress Report 23, 82 p.

Villemin, T., Angelier, J., and Sunwoo, C., 1995, Fractal distribution of fault length and offsets. Implications of brittle deformation evaluation (Lorraine Coal Basin), *in* Barton, C.C., and La Pointe, P.R., eds., Fractal in the Earth Sciences: New York, Plenum Publishing, p. 205–226.

Walsh, J.J., Nicol, A., and Childs, C., 2002, An alternative model for the growth of faults: Journal of Structural Geology, v. 24, p. 1669–1675, doi:10.1016/S0191-8141(01)00165-1.

Walsh, J.J., and Watterson, J., 1988, Analysis of the relationship between the displacements and dimensions of faults: Journal of Structural Geology, v. 10, p. 239–247, doi:10.1016/0191-8141(88)90057-0.

Wells, D.L., and Coppersmith, K.J., 1994. New empirical relationships among magnitude, rupture length, rupture width, rupture area and surface displacement: Bulletin of the Seismological Society of America, v. 84, p. 974–1002.

Wigley, T.M.L., 1973, Chemical solution of the system calcite-gypsum-water: Canadian Journal of Earth Sciences, v. 10, p. 306–315, doi:10.1139/e73-027.

Wilkins, S.J., and Gross, M.R., 2002, Normal fault growth in layered rocks at Split Mountain, Utah. Influence of mechanical stratigraphy on dip linkage, fault restriction and fault scaling: Journal of Structural Geology, v. 24, p. 1413–1429, doi:10.1016/S0191-8141(01)00154-7.

Wong, I.G., and Simon, R.B., 1981, Low-level historical and contemporary seismicity in the Paradox Basin, Utah, and its tectonic implications, *in* Wiegand, D.L., ed., Geology of the Paradox Basin: Denver, Colorado, Rocky Mountain Association of Geologists, p. 169–185.

Wong, I.G., Olig, S.S., and Bott, J.D.J., 1996, Earthquake potential and seismic hazards in the Paradox Basin, southeastern Utah, *in* Huffman, A.C., Jr., Lund, W.R., and Goodwin, L.H., eds., Geology and Resources of the Paradox Basin: Utah Geological Association Guidebook 25, p. 241–250.

Woodhouse, C., Meko, D., MacDonald, G., Stahle, D., and Cook, E., 2010, A 1,200-year perspective of 21st century drought in southwestern North America: Proceedings of the National Academy of Sciences of the United States of America, v. 107, no. 50, p. 21,283–21,288, doi:10.1073/pnas.0911197107.

Woodward-Clyde Consultants, 1980, Geology of the Paradox Basin Study Region: Salt Lake City, Utah, Woodward-Clyde Consultants, prepared for Battelle Memorial Institute, Office of Nuclear Waste Isolation, 125 p.

MANUSCRIPT RECEIVED 24 APRIL 2014
REVISED MANUSCRIPT RECEIVED 19 SEPTEMBER 2014
MANUSCRIPT ACCEPTED 5 NOVEMBER 2014

Printed in the USA